The Footprint of Urban Areas on Global Climate as Characterized by MODIS

MENGLIN JIN

Department of Meteorology, University of Maryland, College Park, College Park, Maryland

ROBERT E. DICKINSON

Earth and Atmospheric Sciences, Georgia Institute of Technology, Atlanta, Georgia

DA-LIN ZHANG

Department of Meteorology, University of Maryland, College Park, College Park, Maryland

(Manuscript received 10 February 2004, in final form 9 August 2004)

ABSTRACT

One mechanism for climate change is the collected impact of changes in land cover or land use. Such changes are especially significant in urban areas where much of the world's population lives. Satellite observations provide a basis for characterizing the physical modifications that result from urbanization. In particular, the Moderate Resolution Imaging Spectroradiometer (MODIS) instrument on the National Aeronautics and Space Administration (NASA) *Terra* satellite measures surface spectral albedos, thermal emissivities, and radiative temperatures. A better understanding of these measurements should improve our knowledge of the climate impact of urbanization as well as our ability to specify the parameters needed by climate models to compute the impacts of urbanization. For this purpose, it is useful to contrast urban areas with neighboring nonurban surfaces with regard to their radiative surface temperatures, emissivities, and albedos. Among these properties, surface temperatures have been most extensively studied previously in the context of the "urban heat island" (UHI). Nevertheless, except for a few detailed studies, the UHI has mostly been characterized in terms of surface air temperatures.

To provide a global analysis, the zonal average of these properties are presented here measured over urban areas versus neighboring nonurban areas. Furthermore, individual cities are examined to illustrate the variations of these variables with land cover under different climate conditions [e.g., in Beijing, New York, and Phoenix (a desert city of the United States)]. Satellite-measured skin temperatures are related to the surface air temperatures but do not necessarily have the same seasonal and diurnal variations, since they are more coupled to surface energy exchange processes and less to the overlying atmospheric column. Consequently, the UHI effects from skin temperature are shown to be pronounced at both daytime and nighttime, rather than at night as previously suggested from surface air temperature measurements. In addition, urban areas are characterized by albedos much lower than those of croplands and deciduous forests in summer but similar to those of forests in winter. Thus, urban surfaces can be distinguished from nonurban surfaces through use of a proposed index formed by multiplying skin temperature by albedo.

1. Introduction

Large modifications of land surfaces occur often through the development of urban areas. These changes modify local climates (Landsberg 1970; Changnon 1978, 1992). Industrialization and population growth have accelerated this impact through expanded human activities and especially land use. Currently, about 2% of the midlatitude land is covered by urban and industrial developments (UNPFA 1999; Jin and Zhang 2002). The net effect of buildings and roads over an area is to replace some of the previous natural or managed vegetation with dry impervious surfaces that alter the exchange of energy and moisture between surface and atmosphere, and in doing so modify surface microclimatic variables such as the temperatures, humidity, and near-surface winds.

Because both nonurban and urban surfaces are quite varied, general statements about how they differ are not readily made. However, temperatures over urban areas are commonly found to be higher than those of outlying rural areas, particularly at night. This elevation of temperatures has been referred to as the "urban heat island" (UHI) (Oke 1982). Many of these previous studies only examined one or a few selected urban ar-

Corresponding author address: Dr. Menglin Jin, Dept. of Meteorology, University of Maryland, College Park, College Park, MD 20742-2425.
E-mail: mjin@atmos.umd.edu

eas (e.g., Bornstern 1968; Karl and Williams 1987; Karl et al. 1988; Huff and Vogel 1978; Changnon 1978; Brest 1987; Gallo et al. 1993; Hansen et al. 2001; Shepherd et al. 2002). Since the effects of urbanization vary from city to city as determined by factors of population density, city size, industrial level, or traffic pattern, knowledge obtained from a few cities may not be valid to be expanded to a global scale. In addition, modifications of clouds and precipitation have also been observed over urban landscapes (King et al. 2003; Ramanathan et al. 2001; Shepherd et al. 2002). Urbanization modifies local climates not only through microclimatology, but also through changes in atmospheric radiation and precipitation as initiated by anthropogenic aerosols. These observed changes have been related to land use, building density, population density, lifestyles, seasons, and prevailing environmental forcing (Oke 1976; 1982; Karl et al. 1988).

Complementary to the previous urban studies are examinations of the role of urbanization on climate from a global perspective as recommended by Houghton et al. (2001). The present paper is intended to further advance the global perspective of urban impacts on climate. Although relatively small in their area, urban environments are distinguished by being where the bulk of the world's population lives, and where many of the world's climate records are taken. Oke (1976) showed that even for a small town of 1000 residents, the typical UHI effect is in the range of 2° to 2.5°C. This has recently been confirmed by Torok et al. (2001), who found that the urban–rural temperature differences may scale with the logarithm of a region's population. Such changes on thermodynamics can modify mesoscale circulations over urban areas (e.g., Wong and Dirks 1978; Yan and Anthes 1988; Avissar and Pielke 1989; Chen and Dudhia 2001).

Although surface air temperatures observed by the World Meteorological Organisation (WMO) have been widely used in the previous UHI studies, changes in sites and instruments as well as irregular coverage (Karl et al. 1988; Peterson 2003) complicate this usage. For example, Peterson (2003) found little differences from the urban–rural temperatures detected at 289 stations and suggested that the urban impact may be at a smaller size than available city and rural stations. Evidently, surface air temperature should be supplemented with other observations to more accurately capture city-induced changes.

Data for skin temperature (T_{skin}) are complementary to those for surface air temperature (T_{air}; Jin et al. 1997; Jin and Dickinson 1999, 2000, 2002; Jin 2000). Because of its weaker coupling to the overlying atmosphere, T_{skin} tends to have a stronger UHI signal than T_{air}. We see its UHI for large cities extend outward from their centers by at least 30 km before becoming undetectable. Nevertheless, the UHI signal from both temperatures varies on daily and seasonal time scales (Roth et al. 1989).

Urban constructions modify surface properties that contribute to the UHI such as albedo and emissivity. Dense distributions of buildings give a "canyon effect" or "cavity effect," where multiple internal reflections resulting from the urban "canopy" geometry reduce surface albedo and emissivity from that of individual flat surfaces (Van de Griend and Owe 1993; Francois et al. 1997; Jin and Liang 2003, manuscript submitted to *J. Climate*, hereafter JL). Using a model framework to describe the effect of the trapping of insolation by tall buildings, Craig and Lowry (1972) found a 20% decrease in daily albedo.

The effects of urbanization are an example of the land cover/use impact on the climate system. The purpose of this study is to utilize the Earth Observing System (EOS) satellite observations to address the following questions: How significant are the UHI effects over different urban areas in terms of T_{skin}? How do the urban developments affect the land surface physical properties (e.g., albedo and emissivity)? The present study makes a first effort to analyze globally the Moderate Resolution Imaging Spectroradiometer (MODIS) land T_{skin}, surface albedo, and emissivity.

Previously, urban effect is reported as urban-to-rural temperature difference, namely urban heat island (Oke 1976, 1982; Landsberg 1970). In this research, instead of studying surface temperature alone, we consider land surface–atmosphere–biosphere as an integrated climate system and analyze various perspectives of urban climate including land surface skin temperature, surface albedo, land surface emissivity, land cover, clouds, and aerosol optical depth of global urban areas. This helps identify surface–atmosphere interactions and simulate urban effects in a global climate model.

It has been argued that urban area, or human impact, is not important as urban regions are only a small portion of land surface. Analyzing urban regions from the globe shows that such an argument is misleading. From observations and from modeling, Vörösmarty et al. (2002) suggested the anthropogenic climate change can have the same magnitude of ENSO. Our research, via satellite observations, proves that land–atmosphere–biosphere interactions cause significant mesoscale circulation anomalies, and these anomalies can propagate to large scale. Global change studies showed that urban areas have larger temperature increase trends than other areas (i.e., "urban warming" Hansen et al. 2001). Therefore, it is essential to better understand urban physical processes in order to better project the future changes of urban climate (Changnon 1992; Houghton et al. 2001).

The next section describes the data sources used for this work. Section 3 presents the evidence of the UHI effects in terms of T_{skin} at the global scale and individual cities, and urban impacts on the surface albedo and emissivity. Section 4 describes a new algorithm that is developed to facilitate the identification of urban areas from satellite observations. Discussion and concluding remarks are given in the final section.

2. Data sources

MODIS is carried on the National Aeronautics and Space Administration's (NASA's) *Terra* satellite launched in May 2000, and later on the *Aqua* satellite that is too recent to be used here. On *Terra*, it measures the earth's surface characteristics through seven solar and three thermal spectral bands at 1030 LT and 2230 LT daily. Each pixel has a 1-km resolution at the nadir (Wan and Dozier 1996) and is scaled up to a 5-km resolution in this study. The satellite-measured T_{skin} is derived from longwave bands that detect surface emissions. Its value depends on surface energy budget and so provides an observational constraint on the balance between net surface radiation and fluxes of energy and water (Jin et al. 1997; Jin and Dickinson 1999, 2000). Only the measured values with quality flags attesting to the absence of clouds are used. The MODIS spectral emissivities are converted into broadband values using the moderate resolution transmittance (MODTRAN) algorithm (see JL). The MODIS provisional land cover product with a 5-km resolution is used herein to categorize the land surface according to the International Geosphere–Biosphere Project (IGBP) 17 land cover types (Friedl et al. 2002), as given in Table 1.

An urban category has been obtained from MODIS version-4 observations (Schneider et al. 2002). Previous MODIS land cover data used the Digital Chart of the World urban data that were originally digitized from Operational Navigation and Jet Navigation Charts by the U.S. Defense Mapping Agency (Danko 1992); it is available from the U.S. Geological Survey's National Center for Earth Resources Observation and Science (EROS) Data Center (EDC). Unfortunately, many of the base maps used the urban data from the 1960s and 1970s, and they are inconsistent globally and do not include new cities or new urban development in recent decades (M. Fridel and A. Schneider 2004, personal communication). In recent MODIS retrievals, such data have been updated for recent trends in urbanization to provide quantitative measures of urban properties that are of importance for climate studies.

TABLE 1. Global land cover index (available online at http://geography.bu.edu/landcover/userguidelc/consistent.htm).

	Land cover index
1.	Evergreen needleleaf
2.	Evergreen broadleaf
3.	Deciduous needleleaf
4.	Deciduous broadleaf
5.	Mixed forest
6.	Closed shrubland
7.	Open shrubland
8.	Woody savanna
9.	Savanna
10.	Grasslands
11.	Permanent wetlands
12.	Cropland
13.	Urban
14.	Cropland/natural vegetation
15.	Snow and ice
16.	Barren
17.	Water

We used MOD43B3 albedo product, which is derived from the *Terra* MODIS instrument in 16-day, L3 global, 5-km ISIN projection (Schaaf et al. 2002). Albedo is the ratio of upwelling to downwelling radiative flux at the surface. Downwelling flux is the sum of two parts: the direct part and diffuse part. Albedo in the absence of a diffuse part is the so-called black-sky albedo (directional hemispherical reflectance), which is a function of solar zenith angle. Albedo in the absence of a direct part when the diffuse component is isotropic is defined as the white-sky albedo (bihemispherical reflectance). Black-sky and white-sky albedos are the extreme cases of completely direct and completely diffuse situations. Actual albedo is a value between these two as determined by atmospheric aerosol condition.

3. Results

In this section, the regional and global occurrences of UHI are first demonstrated using the satellite-measured T_{skin}. Then, surface albedo and emissivity over urban areas are examined to clarify the reasons for the UHI occurrences. Finally, an "urban index" is proposed to identify urban regions using satellite-observed information.

a. The urban heat island

This work intends to examine the urban effect in skin temperature field. In order to reduce the natural elevation impact, we have tried to remove those surrounding pixels far higher or lower than the urban pixel, through the use of 1-km elevation data currently used as boundary condition for the land surface model in National Center of Atmosphere Research.

The global latitudinal distribution urban nocturnal T_{skin} and diurnal range are shown in Fig. 1. Cities are concentrated between 30° and 65°N in the Northern Hemisphere, with much fewer cities in the Tropics and in midlatitudes in the Southern Hemisphere, where the earth surface is mostly covered by water. Significant longitudinal variations in urban T_{skin} are seen corresponding to the north–south distribution of net radiation received at the earth's surface. In this figure, cloud contamination is minimized through the use of clear days. Thus, the indicated variability of T_{skin} depends on factors such as variation in absorption of solar radiation, variation in elevation, nearness of oceanic influences, and dryness of the underlying surfaces. The largest range at 30°N of more than 30°C occurs where the largest fraction of land is covered by deserts. Similarly, the diurnal range (Fig. 1b) over the same latitude differs significantly, largely determined by the local or regional sky conditions and surrounding surface land cover.

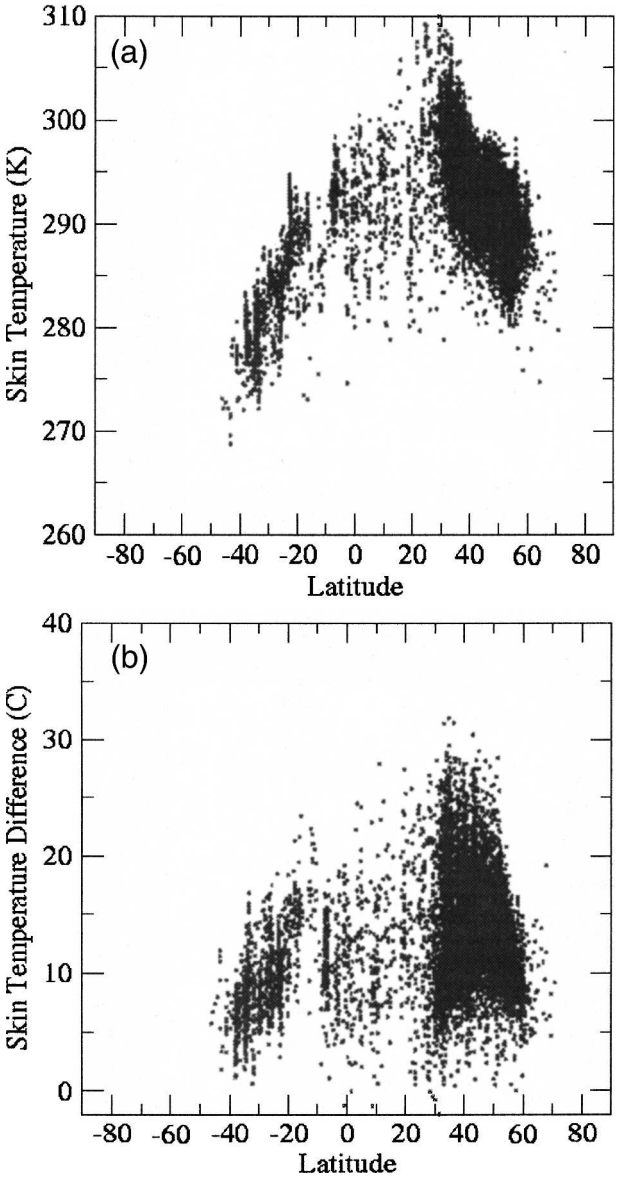

FIG. 1. (a) Longitudinal variation of monthly mean nocturnal urban T_{skin} for the month of Jul 2001. Urban areas are obtained from the MODIS data, while T_{skin} are obtained from the MODIS data at a 5-km resolution. (b) Similar to (a) except that this is the diurnal range for each urban pixel. The range is calculated from monthly daytime T_{skin} minus monthly mean nighttime T_{skin}.

On average, the urban T_{skin} are 1°–5°C higher than those over croplands, with larger differences during nighttime in the Southern (winter) Hemisphere (Fig. 2b). By comparison, the daytime T_{skin} differences between the urban areas and adjacent croplands are small but still detectable, especially in the ranges of 10°S–40°N and 30°–45°S (Fig. 2a). Cities at high latitudes in the Northern Hemisphere (e.g., 55°–60°N) are even cooler than the rural areas during daytime. Large T_{skin} differences are also notable at the desert latitudes of 15°–25°N and 10°–20°S because T_{skin} in desert cities are close to those in their surrounding deserts but higher than those in their nearby croplands. A large drop in urban T_{skin} occurs near 15°N, at which latitude few cities are located. The amplitude of diurnal T_{skin} changes is small (<10°C) in the Tropics and Southern Hemisphere where oceanic influences are most pronounced, whereas it is large (>30°C) at middle to high latitudes in the Northern Hemisphere.

The differences between the urban and forest regions over subtropical and middle latitudes of the Northern Hemisphere are about 4°C (Fig. 3) with extremes up to 12°C at around 22°N. Urban differs more from forests during the day than it does at night.

Three examples of major cities are examined in this study, namely, two large metropolitan cities in developed and developing countries (i.e., New York, New York, and Beijing, China) and one city with extreme natural (desert) conditions (i.e., Phoenix, Arizona). As shown in Fig. 4a, the city of Beijing is surrounded mostly by cropland, except to its west (cf. Fig. 4a and Table 1); its northwest–southeast orientation reflects its urban expansion to Tianjin, which is one of the most rapidly growing coastal cities in China. High skin temperatures are evident over Beijing during both the daytime and nighttime of January and July (see Figs. 4b,c). The MODIS data show more pronounced UHI effects over the southern part of the city where its building density is higher than over its northern part with its more widely spaced buildings such as universities, research institutions, and government offices, as well as parks and lakes. The *Weekly Weather & Crop Bulletin* shows for this month little rainfall across most of the North China Plain, including the Beijing metropolitan area. Presumably more irrigation than normal was needed as a response, possibly amplifying the daytime urban–rural contrast at that time and hence weakening the day–night contrasts (cf. Figs. 4c,d). The July nighttime T_{skin} of Beijing was only elevated with respect to the eastern cropland but not relative to the western forest mountains (see Fig. 4d).

To exclude the influence of the latitudinal variation of solar insolation at different latitudes, Fig. 5 compares urban T_{skin} longitudinally to the adjacent rural areas over a spatial scale of 200 km for the city of New York. Its UHI effects are visible in January during both daytime and nighttime (cf. Figs. 5a,b). New York, as an east coast city, has relatively small diurnal changes of T_{skin}, as compared to Beijing, but it is warmer than the adjacent pixels to the west during both the daytime and nighttime. The nocturnal T_{skin} decreases steeply going inland in winter, for example, as much as 5°C across the 200-km range, whereas in daytime or in summer, there is a more flat change of about 2°C.

Because the city of Phoenix, the 17th largest city of the United States, has more vegetation than its surrounding areas, its T_{skin} is substantially lower during both the day and nighttime (see Figs. 6a,b). The coldest

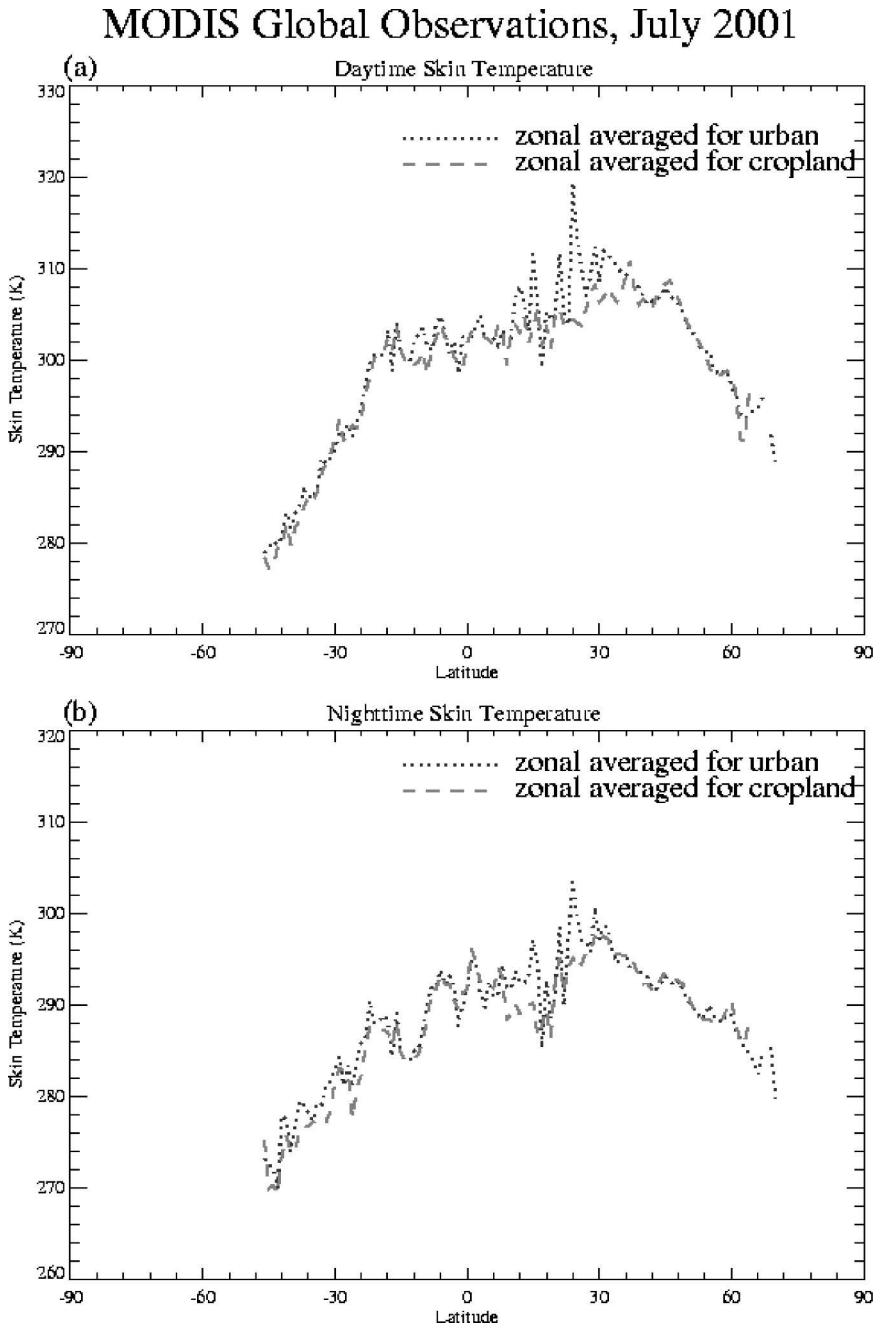

FIG. 2. Comparison of the monthly and zonal averaged T_{skin} between the urban surfaces and surrounding croplands: (a) daytime and (b) nighttime, for the month of Jul 2001.

pixel to the west of the city (i.e., 314 K by day and 296 K at night) occurs over local mountains, but its UHI effects are barely detectable in January for either day or night.

b. Urban effects on surface albedo and emissivity

Urban construction reduces both albedo and emissivity (Figs. 7a,b). Figure 7a compares the zonal averaged urban albedo to the averaged cropland albedo between 30° and 65°N, where most cities are located. City albedo values are 2%–5% smaller than those in the adjacent croplands, as noted earlier, for example, by Brest (1987). The largest urban albedos are observed over the desert areas around 30°N and accompanied by high daytime and nighttime T_{skin} (see Fig. 6). Surface emissivity is about 1%–2% lower than that of

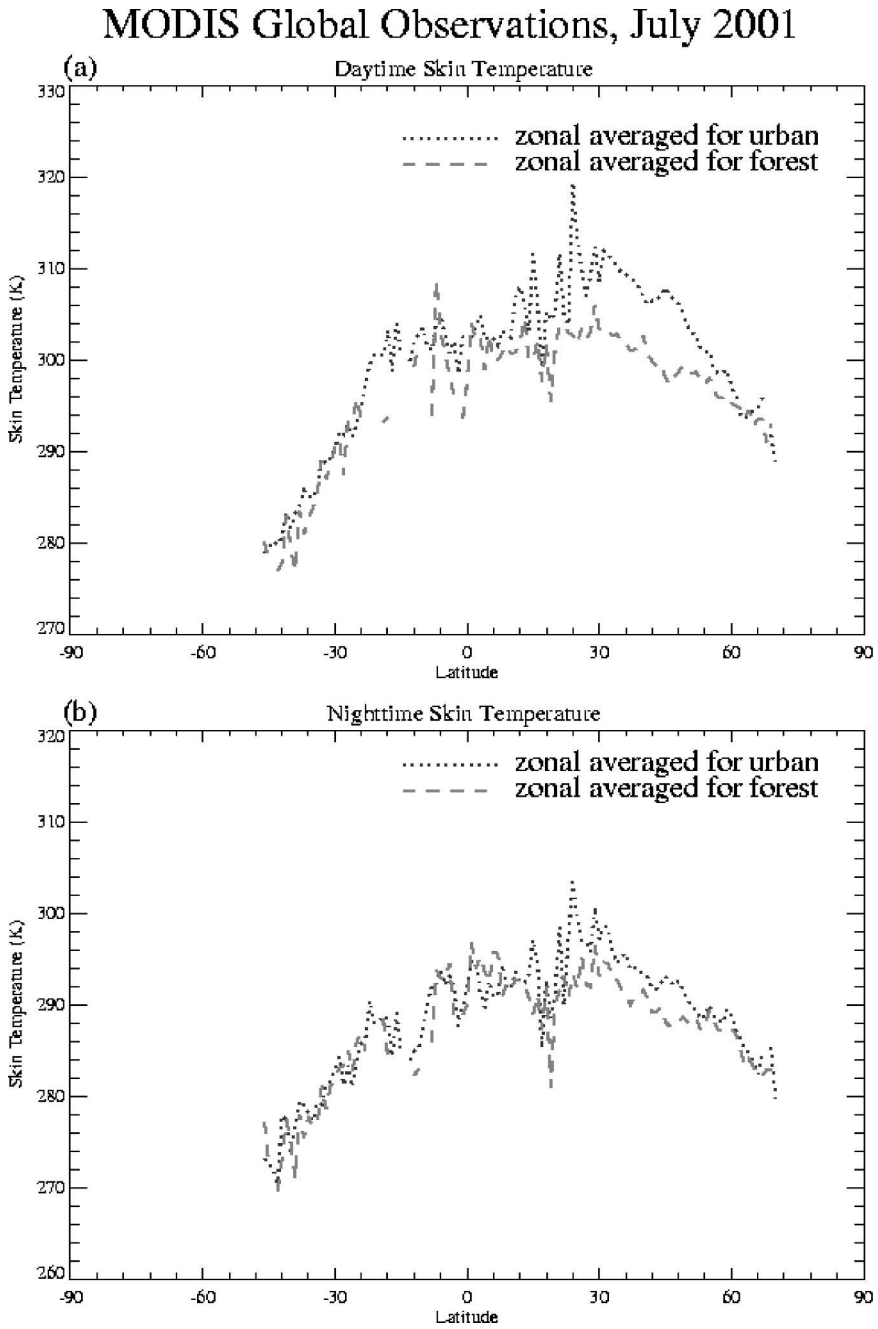

FIG. 3. Same as in Fig. 2, but for T_{skin} between the urban surfaces and surrounding forests. The forests are near (100 km) the urban regions.

nearby croplands (Fig. 7b). The spatial distributions of albedo and emissivity for Beijing are given in Fig. 8, which shows that the southern part of the city has albedo lower than 0.12 and emissivity lower than 0.94, that is, 3% less than the emissivity of the surrounding regions.

Albedo is determined by MODIS as a weighted average of spectral albedos at seven different wavelengths. For use in climate models, they are divided into visible and near-infrared (NIR) wavelengths. Further insights are provided herein as to the difference between urban and nonurban areas and how it is distributed spectrally through Figs. 9, 10, and 11, using the city of New York as an example. The longitudinal distribution of total albedo is compared in Fig. 9 with its component visible and near-infrared broadbands, which indicates that the urban and nonurban difference is largely from the near-infrared differences. This dis-

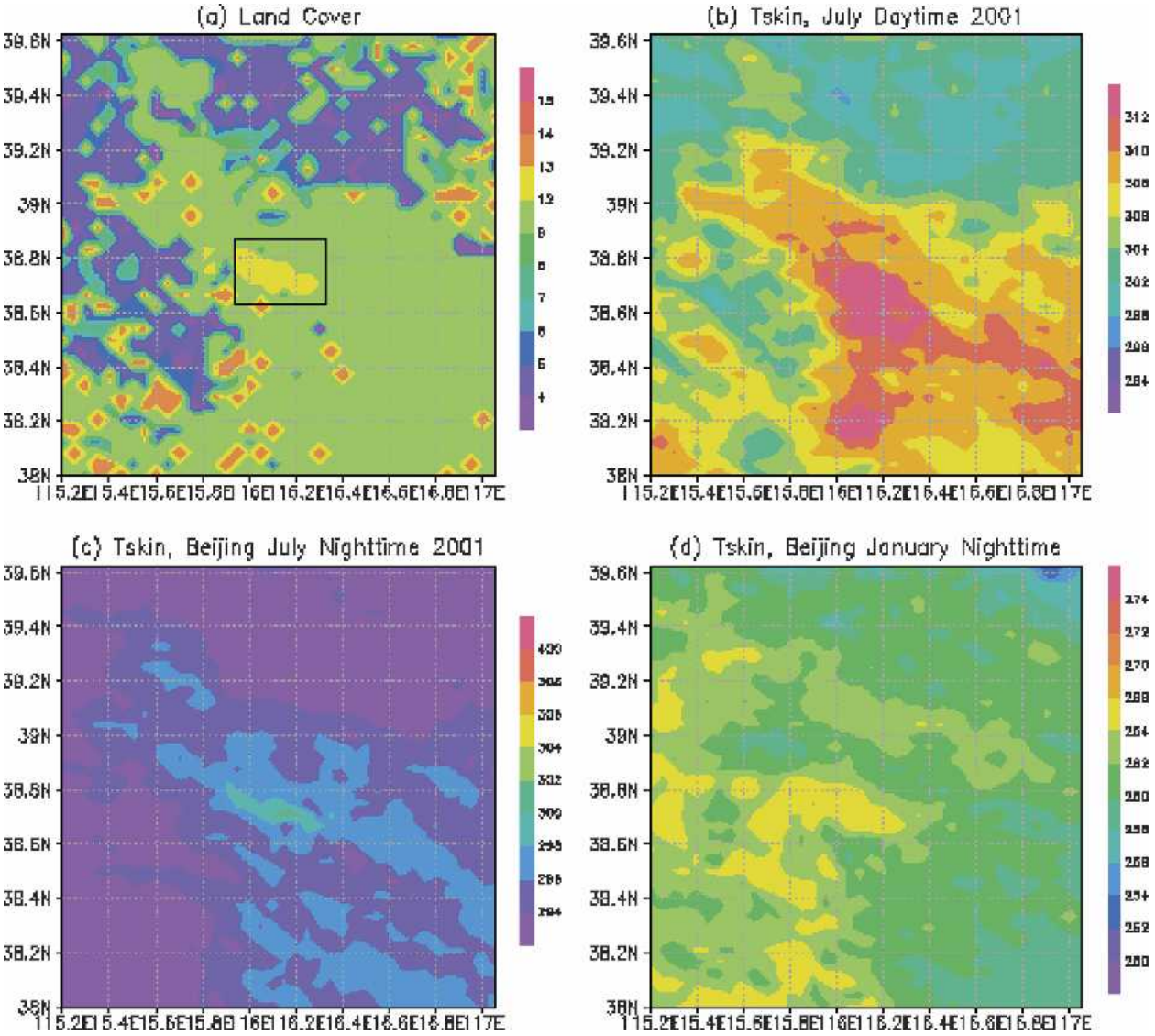

FIG. 4. (a) Horizontal distribution of the land cover indices (see Table 1) over Beijing and its neighboring area, obtained from the MODIS land cover product. Each grid is 5 km × 5 km. (b) Horizontal distribution of the monthly mean daytime skin temperature (k) over Beijing and its surroundings for the month of Jul 2001. (c) Same as in (b), but for the nighttime T_{skin}. (d) Same as in (b), but for the nighttime skin T_{skin} for the month of Jan 2001.

tinction is further seen in Fig. 10, which shows averages over the urban area versus nearby cropland and deciduous forest. Two differences are evident: (a) the relative changes in the NIR are larger than in the visible (about 25% versus about 10%), and (b) the NIR albedo is nearly an order of magnitude larger than the visible albedo. In other words, the urban and rural visible albedos are both about 0.04, whereas the urban NIR albedo is 0.27 compared to about 0.32 for cropland and forest. The shortwave broadband albedo, which is approximately an average of the visible and NIR broadband albedos, is about 0.15 for urban and 0.18 for cropland and forest.

Figure 11 presents the spectral variations of albedo and the contrasts between winter and summer. We have only sampled snow-free and cloud-free pixels, and thus the seasonality is largely from changes in the sun angle, browning and drop of leaves, and more exposure of bare soil. In general, urban albedo varies significantly with wavelength, with higher albedo in NIR and lower albedo in the visible in both July and January. In July, the peak difference occurs at 0.9 μm, with an urban value of 0.34 and cropland and forest values higher than 0.4. In January, the contrasts are smaller and the peak difference occurs at 1.2 μm.

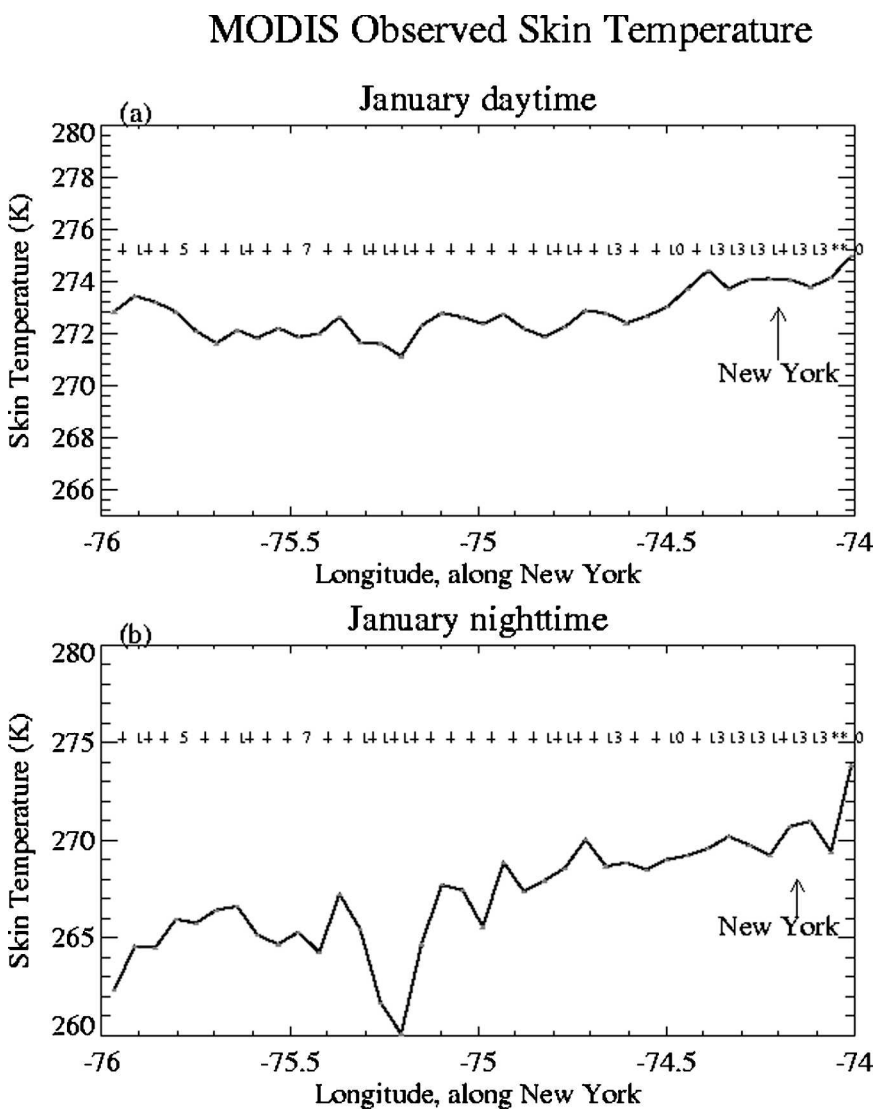

FIG. 5. The zonal distribution of monthly averaged T_{skin} and land cover for each pixel through the latitude of New York City: (a) daytime and (b) nighttime for the month of Jan 2001. Land cover information for each pixel (at 5 km) is given as ASCII values in the plot. Index of 13 denotes the urban coverage; see Table 1 for the definition of other land cover indices.

4. The urban index

Urban areas have generally been determined from satellite data from the nighttime lighting. Such a measure is more an index of electricity use than of the urban features that are significant for climate study. For such purposes, indices are needed that are related to the mechanisms by which urban areas modify climate. We find that urban areas can usefully be characterized by combining skin temperature and albedo (α_i), that is,

$$\mathrm{UI}_i = (1 - \alpha_i)T_{\text{skin-}i}, \quad (1)$$

where UI represents the urban index, and the subscript i denotes each pixel.

Figure 12 compares the UHI structures of New York and its surrounding regions analyzed using T_{skin} to those using the UI. Because of their large T_{skin}, the cities of New York, Washington, D.C., and Philadelphia, Pennsylvania, are already well identified from the T_{skin} map (see Fig. 12a). However, as shown for Phoenix, some urban areas have similar T_{skin} to their surrounding rural regions so that T_{skin} alone is not a reliable index. With the UI, the three eastern U.S. urban areas are easily detected by higher UI values than their neighboring nonurban regions. Similarly, the urban index for Beijing shows a more realistic size and spatial spread of Beijing than its original MODIS land cover data (cf. Figs. 4a and 13).

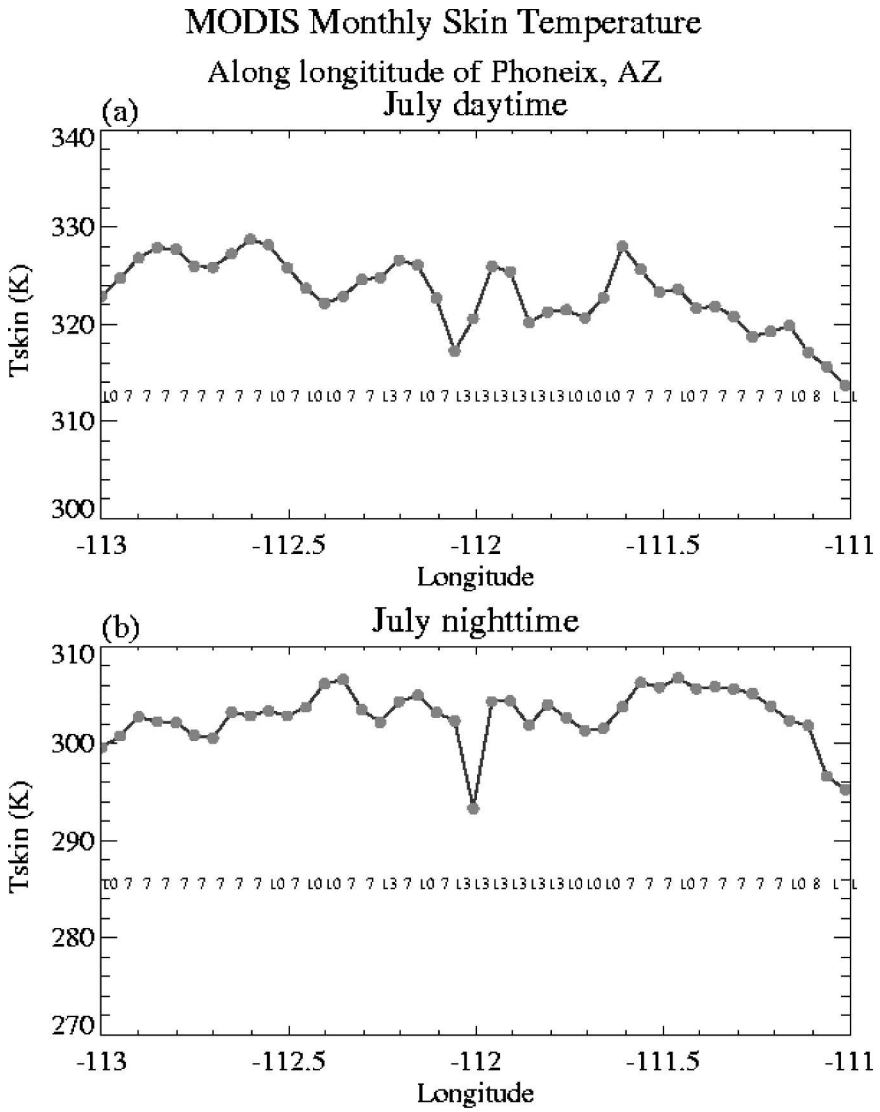

FIG. 6. Same as in Fig. 5, but for Phoenix, AZ.

Thus, the UI provides a physically based urban mapping approach to distinguishing urban from rural areas. Further development using the general principals behind the index presented here should eventually provide a robust, well-validated measure of urban intensities from the viewpoint of climate modeling.

5. Discussion and concluding remarks

In this study, the EOS satellite-measured skin temperatures are used to identify globally the urban areas in order to evaluate the human impact on the earth's climate system. The UHI effects are found in terms of skin temperature anomalies both locally for a few selected cities and globally, and in all seasons and at both the daytime and nighttime. Previous studies emphasized the UHI effects in terms of surface air temperature at night during summer when surface winds are light.

In this paper, we have shown through a global analysis of satellite data that T_{skin} is mostly but not always larger in urban areas than in surrounding rural areas. Urban areas have a wide variety of surfaces including many of those present in the rural areas. Thus, it is not possible to make a generalization that compares all urban with all rural areas. However, cities are distinguished by their large fraction of mostly dark impervious areas, often asphalt. These surfaces introduce into urban environments distinctly higher Bowen ratios and lower albedos and emissivities. The daytime sensible heat fluxes of moist areas are typically less than half of

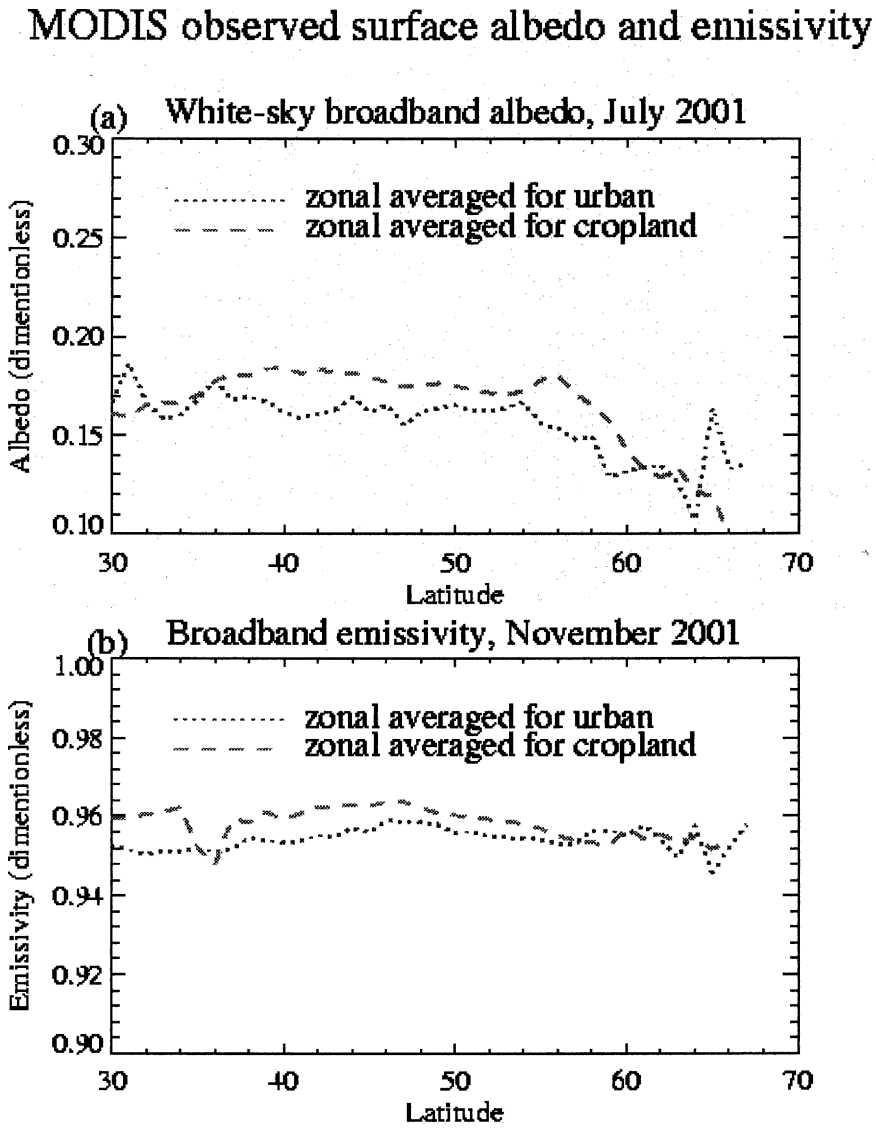

FIG. 7. Monthly and zonal averaged (a) surface albedo for the month of Jul 2001 and (b) surface emissivity for the month of Nov 2001 in the latitudes of 30°–70°N over urban areas (dotted lines) and their adjacent croplands (dashed lines).

the latent fluxes, so with a large impervious fraction, the sensible fluxes and hence the daytime boundary layer warming may be nearly doubled. With higher Bowen ratios, the fraction of net daytime radiation being stored is also comparably larger, leading to warmer nighttime temperatures. This fraction of impervious area is the primary distinction between urban and forest surfaces, which indeed have overall albedos slightly lower than urban ones. Shorter vegetation has higher and smoother albedos, amplifying their surface temperature diurnal range from that of the rougher cities and forests, since their atmospheric surface boundary layers respond with larger temperature gradients for the same daytime heating and nighttime cooling. Their albedo difference overall makes them cooler than urban areas, but concentrated at night when the effect of surface roughness is additive rather than canceling the albedo difference (being realized to some degree at night through less storage of the rural surface). Our examination of Beijing illustrated the differences from the urban region with both nearby forests and croplands.

In addition to surface albedo and emissivity, the temperature differences between urban and rural forest regions also result from lower leaf temperature and more active transport of forests due to large roughness length.

Most UHI studies have been in moist midlatitude cities. In dry regions, the Bowen ratios are generally larger in the rural areas as the cities have more

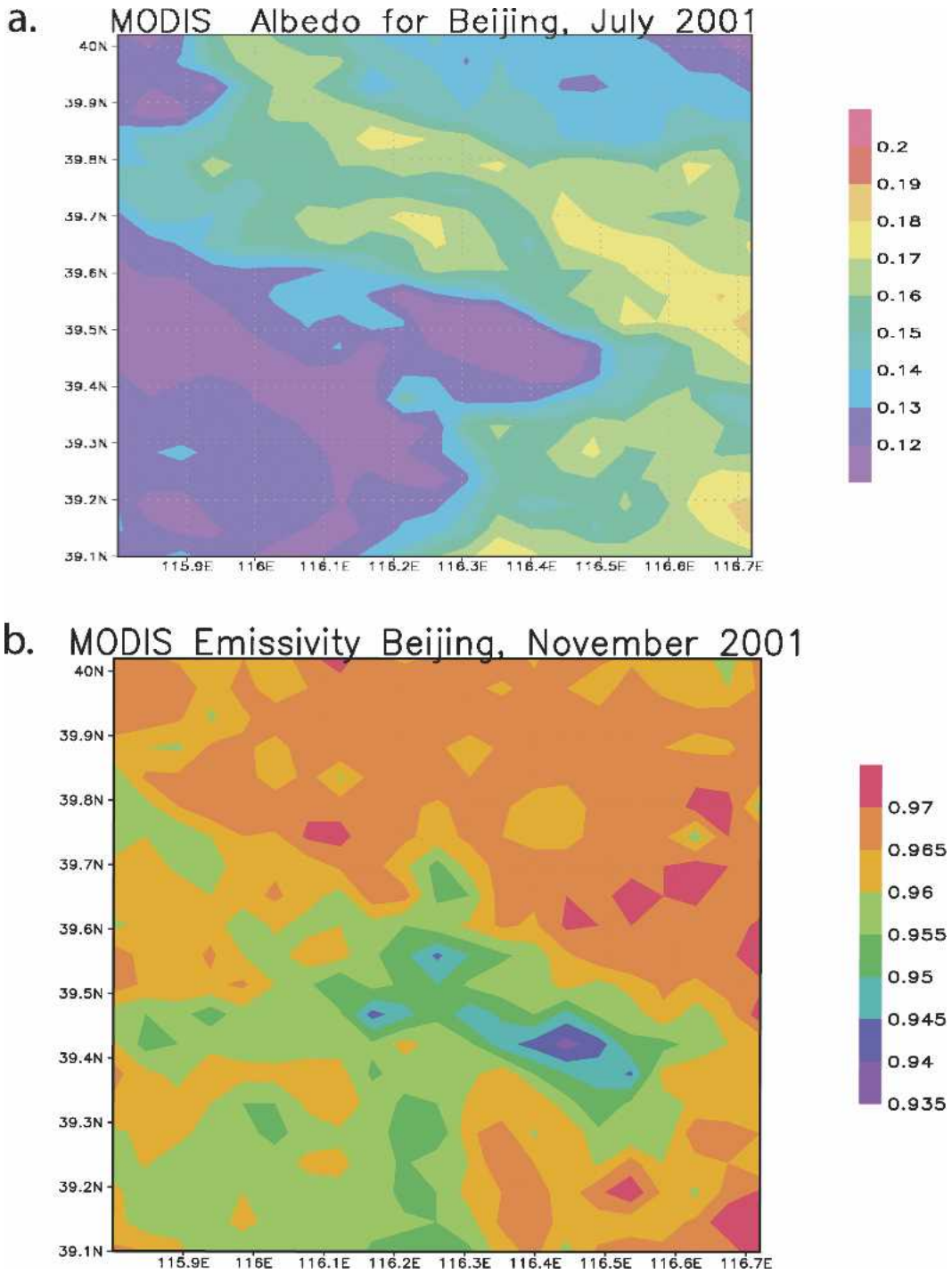

FIG. 8. (a) Spatial variation of the monthly mean surface albedo over Beijing and its surroundings for the month of Jul 2001. (b) Spatial distribution of the monthly mean surface emissivity over Beijing and its surroundings for the month of Nov 2001.

vegetation, and the effects described above are reversed. However, the urban areas will have compensating lower albedos. Our analysis of Phoenix indicates little distinction between the city and its surroundings, possibly a general result for semiarid and arid regions.

The MODIS results presented herein have important implications with respect to the modeling of land sur-

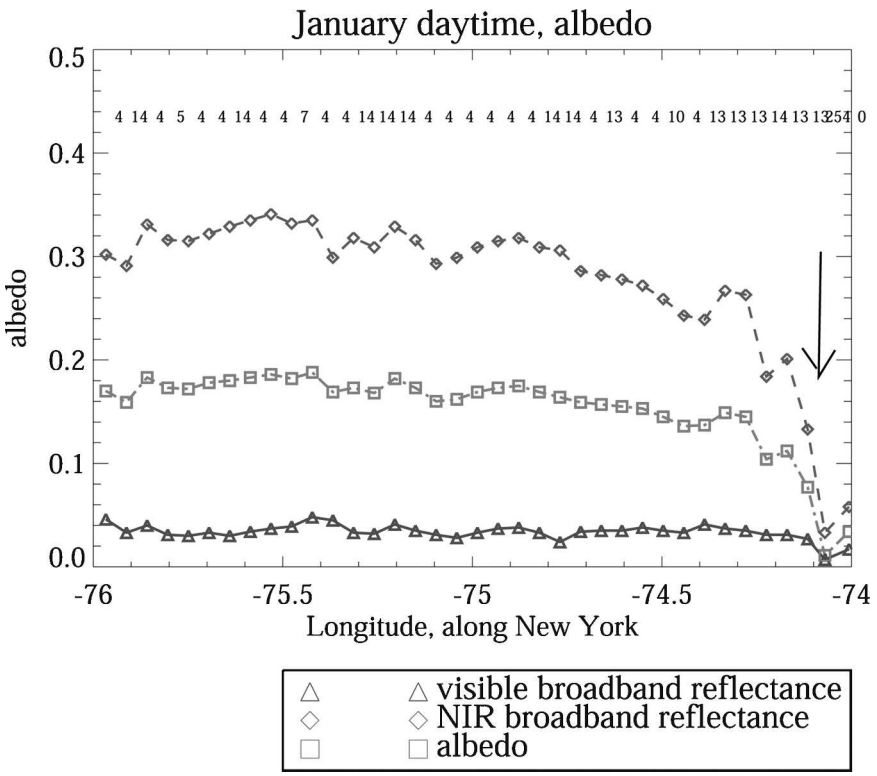

FIG. 9. Same as in Fig. 5, but for the surface shortwave, NIR, and visible broadband albedos. The arrow links the urban pixels (category 13) with the corresponding abrupt decrease on reflectance.

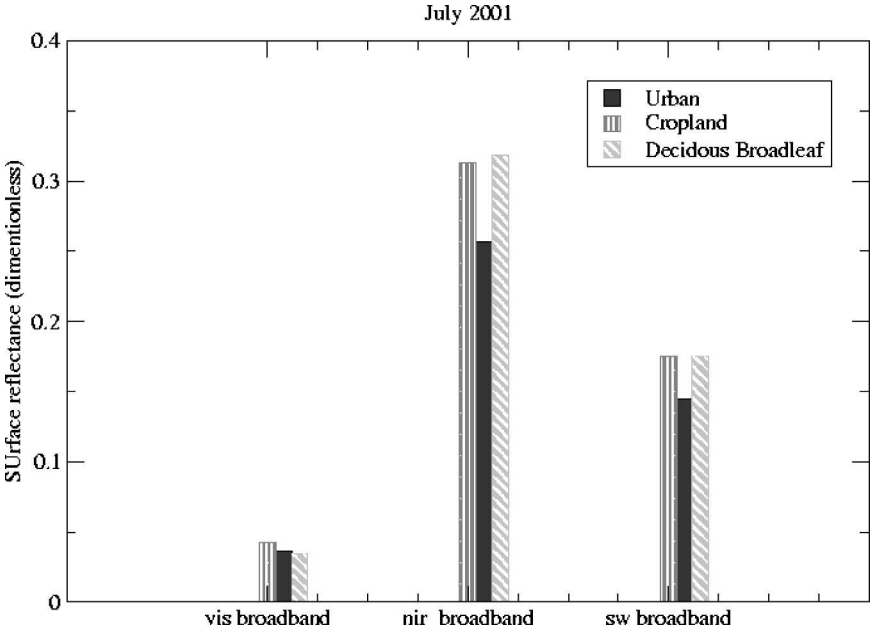

FIG. 10. Comparisons of visible broadband (VIS), NIR, and shortwave broadband (SW) albedos for urban, cropland, and deciduous broadleaf land cover over New York and the surrounding regions.

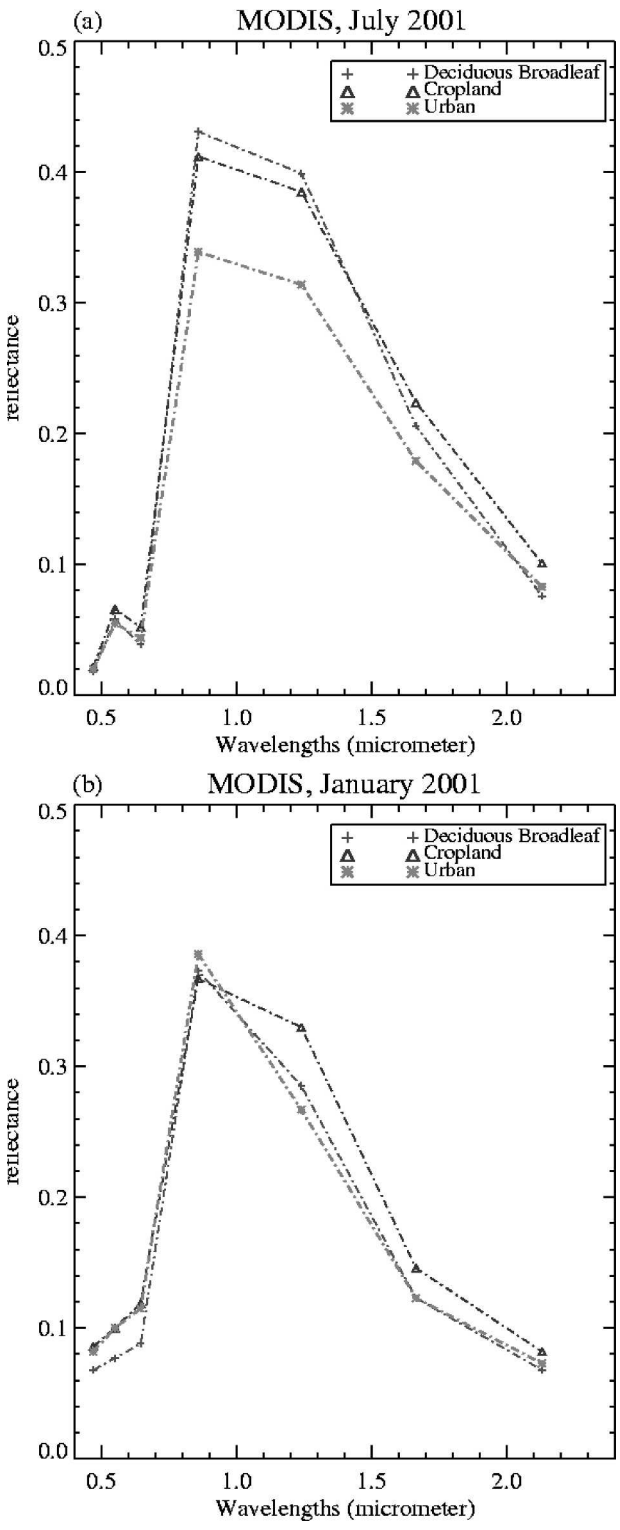

FIG. 11. The spectral albedo for urban, cropland, and deciduous broadleaf from MODIS, for New York and the surrounding regions, as in Figs. 10 and 12, for (a) Jul and (b) Jan.

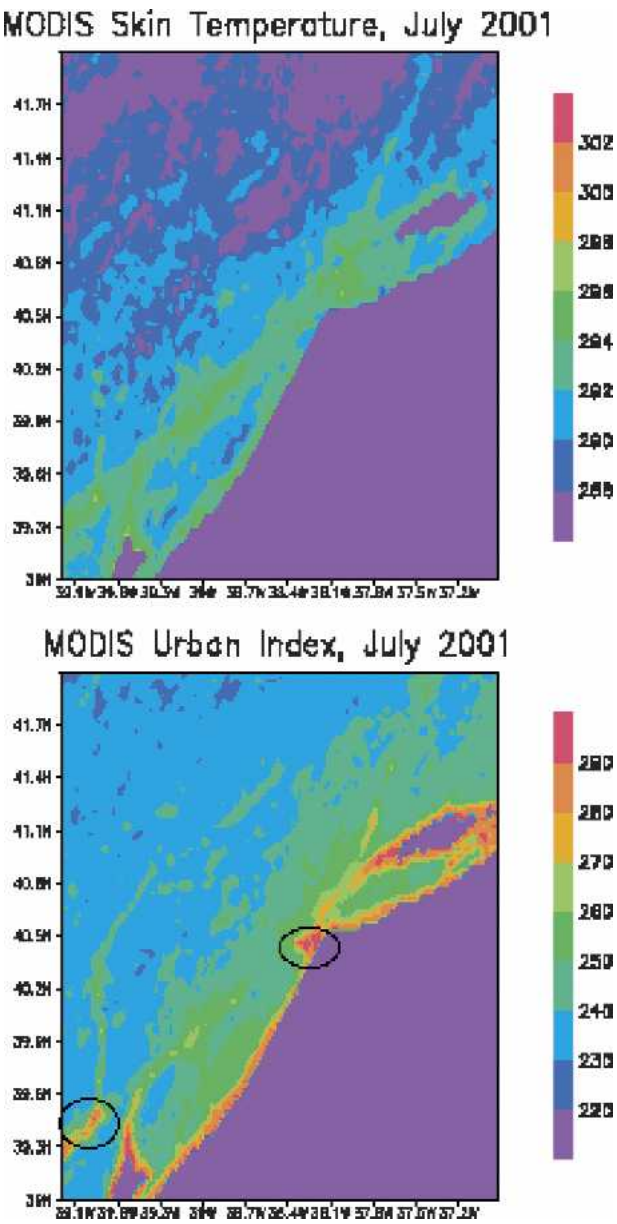

FIG. 12. Urban index for Jul 2001 for New York and its surrounding areas: (a) T_{skin} and (b) the corresponding urban index. The circled areas in (b) show the urban characteristics of New York and Washington, DC, better than those in (a).

face processes for climate change. Specifically, high-resolution satellite observations of the surface albedo, emissivity, and land cover could be used to update the land surface parameters for both numerical weather prediction and global (regional) climate models (e.g., JL). The effect of urban areas on the regional climate system occurs through the land surface–atmosphere interactions. Beside the effects described here, urban areas are known to modify the distribution of aerosol, clouds, and rainfall (King et al. 2003; Shepherd et al. 2002). Climate models may provide a good approach

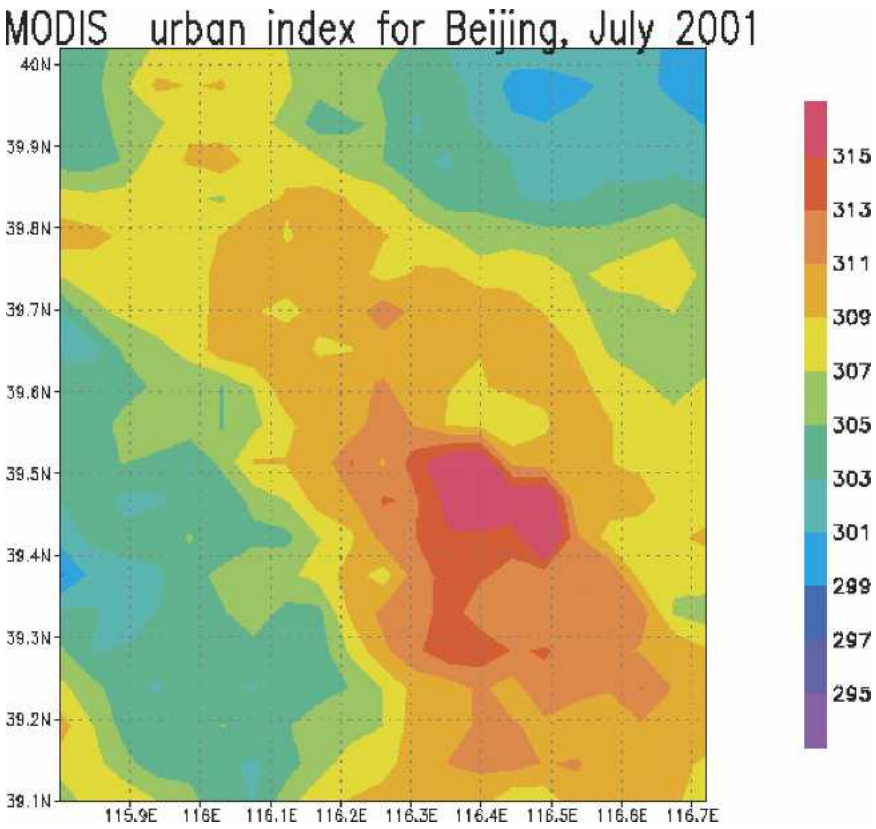

FIG. 13. Urban index over Beijing and its surrounding areas for the month of Jul 2001.

for assessing the global consequences of the urban climate modifications.

Acknowledgments. We thank Dr. Zhengmin Wan and Dr. Feng Gao for kindly preparing the MODIS land surface data for this study. Special thanks go to Dr. Michael D. King of the NASA Goddard Space Flight Center for his helpful discussions on the MODIS reflectance and albedo retrieval. This work was funded by NASA's EOSIDS project.

REFERENCES

Avissar, R., and R. A. Pielke, 1989: A parameterization of heterogeneous land surfaces for atmospheric numerical models and its impact on regional meteorology. *Mon. Wea. Rev.,* **117,** 2113–2136.

Bornstern, R. D., 1968: Observations of the urban heat island effect in New York City. *J. Appl. Meteor.,* **7,** 575–582.

Brest, C. L., 1987: Seasonal albedo of an urban/rural landscape from satellite observations. *J. Climate Appl. Meteor.,* **26,** 1169–1187.

Changnon, S. A., Jr., 1978: Urban effects on severe local storms at St. Louis. *J. Appl. Meteor.,* **17,** 578–592.

——, 1992: Inadvertent weather modification in urban areas: Lessons for global climate change. *Bull. Amer. Meteor. Soc.,* **73,** 619–627.

Chen, F., and J. Dudhia, 2001: Coupling an advanced land surface–hydrology model with the Penn State–NCAR MM5 modeling system. Part II: Preliminary model validation. *Mon. Wea. Rev.,* **129,** 587–604.

Craig, C. D., and W. P. Lowry, 1972: Reflections on the urban albedo. Preprints, *Conf. on the Urban Environment and Second Conf. on Biometeorology*, Philadelphia, PA, Amer. Meteor. Soc., 159–164.

Danko, D. M., 1992: The Digital Chart of the World project. *Photogramm. Eng. Remote Sens.,* **58,** 1125–1128.

Francois, C., C. Ottle, and L. Prevot, 1997: Analytical parameterization of canopy directional emissivity and directional radiance in the thermal infrared. Application on the retrieval of soil and foliage temperatures using two directional measurements. *Int. J. Remote Sens.,* **18,** 2587–2621.

Friedl, M. A., and Coauthors, 2002: Global land cover mapping from MODIS: Algorithms and early results. *Remote Sens. Environ.,* **83,** 287–302.

Gallo, K. P., A. L. Mcnab, T. R. Karl, J. F. Brown, J. J. Hood, and J. D. Tarpley, 1993: The use of NOAA AVHRR data for assessment of the urban heat island effect. *J. Appl. Meteor.,* **32,** 899–908.

Hansen, J., R. Ruedy, M. Sato, M. Imhoff, W. Lawrence, D. Easterling, T. Peterson, and T. Karl, 2001: A closer look at United States and global surface temperature change. *J. Geophys. Res.,* **106** (D20), 23 947–23 963.

Houghton, J. T., Y. Ding, D. J. Griggs, M. Noguer, P. J. van der Linden, X. Dai, K. Maskell, and C. A. Johnson, Eds., 2001: *Climate Change 2001: The Scientific Basis*. Cambridge University Press, 881 pp.

Huff, F. A., and J. L. Vogel, 1978: Urban, topographic and diurnal effects on rainfall in the St. Louis region. *J. Appl. Meteor.,* **17,** 565–577.

Jin, M., 2000: Interpolation of surface radiation temperature mea-

sured from polar orbiting satellites to a diurnal cycle. Part 2: Cloudy-pixel treatment. *J. Geophys. Res.,* **105** (D3), 4061–4076.

——, and R. E. Dickinson, 1999: Interpolation of surface radiation temperature measured from polar orbiting satellites to a diurnal cycle. Part 1: Without clouds. *J. Geophys. Res.,* **104,** 2105–2116.

——, and ——, 2000: A generalized algorithm for retrieving cloudy sky skin temperature from satellite thermal infrared radiances. *J. Geophys. Res.,* **105** (D22), 27 037–27 047.

——, and ——, 2002: New observational evidence for global warming from satellite. *Geophys. Res. Lett.,* **29,** 1400, doi:10.1029/2001GL013833.

——, and D.-L. Zhang, 2002: Changes and interactions between skin temperature and leaf area index in summer 1981–1998. *Meteor. Atmos. Phys.,* **80,** 117–129.

——, R. E. Dickinson, and A. M. Vogelmann, 1997: A Comparison of CCM2–BATS skin temperature and surface-air temperature with satellite and surface observations. *J. Climate,* **10,** 1505–1524.

Karl, T. R., and C. N. Willams Jr., 1987: An approach to adjusting climatological time series for discontinuous inhomogeneities. *J. Climate Appl. Meteor.,* **26,** 1744–1763.

——, H. F. Diaz, and G. Kukla, 1988: Urbanization: Its detection and effect in the United States Climate Record. *J. Climate,* **1,** 1099–1123.

King, M. D., and Coauthors, 2003: Cloud and aerosol properties, precipitable water, and profiles of temperature and humidity from MODIS. *IEEE Trans. Geosci. Remote Sens.,* **41,** 442–458.

Landsberg, H. E., 1970: Man-made climatic changes. *Science,* **170,** 1265–1274.

Oke, T. R., 1976: City size and the urban heat island. *Atmos. Environ.,* **7,** 769–779.

——, 1982: The energetic basis of the urban heat island. *Quart. J. Roy. Meteor. Soc.,* **108,** 1–24.

Peterson, T. C., 2003: Assessment of urban versus rural in situ surface temperatures in the contiguous United States: No difference found. *J. Climate,* **16,** 2941–2959.

Ramanathan, V., P. J. Crutzen, J. T. Kiehl, and D. Rosenfeld, 2001: Aerosols, climate, and the hydrological cycle. *Science,* **294,** 2119–2124.

Roth, M., T. R. Oke, and W. J. Emery, 1989: Satellite-derived urban heat islands from three costal cities and the utilization of such data in urban climatology. *Int. J. Remote Sens.,* **10,** 1699–1720.

Schaaf, C. B., and Coauthors, 2002: First operational BRDF, Albedo and Nadir reflectance products from MODIS. *Remote Sens. Environ.,* **83,** 135–148.

Schneider, A., M. A. Friedl, D. K. McIver, and C. E. Woodcock, 2002: Mapping urban areas by fusing multiple sources of coarse resolution remotely sensed data. *Photogramm. Eng. Remote Sens.,* **69,** 1377–1386.

Shepherd, J. M., H. Pierce, and A. J. Negri, 2002: Rainfall modification by major urban areas: Observations from spaceborne rain radar on the TRMM satellite. *J. Appl. Meteor.,* **41,** 689–701.

Torok, S. J., J. G. Morris, C. Skinner, and N. Plummer, 2001: Urban heat island features of southeast Australian towns. *Aust. Meteor. Mag.,* **50,** 1–13.

UNPFA, 1999: *The State of World Population 1999*. United Nations Population Fund, United Nations Publications, 76 pp.

Van de Griend, A., and M. Owe, 1993: On the relationship between thermal emissivity and the normalized difference vegetation index for nature surfaces. *Int. J. Remote Sens.,* **14,** 1119–1131.

Vörösmarty, C. J., P. Green, J. Salisbury, and R. B. Lammers, 2000: Global water resources: Vulnerability from climate change and population growth. *Science,* **289,** 284–288.

Wan, Z., and J. Dozier, 1996: A generalized split-window algorithm for retrieving land-surface temperature from space. *IEEE Trans. Geosci. Remote Sens.,* **34,** 892–904.

Wong, K. K., and R. A. Dirks, 1978: Mesoscale perturbations on airflow in the urban mixing layer. *J. Appl. Meteor.,* **17,** 677–688.

Yan, H., and R. A. Anthes, 1988: The effect of variation in surface moisture on mesoscale circulations. *Mon. Wea. Rev.,* **116,** 192–208.